Nucleic Acids Research, 2026, **54**, gkag270
https://doi.org/10.1093/nar/gkag270
Nucleic Acid Enzymes

Delineation of a novel assembly intermediate in Rous sarcoma virus integration pathway

Rahul Chadda [1,2], Sibes Bera [3,4], Mohamed Ghoneim [1,5], Tamara De Melo [3], Duane P. Grandgenett [3], Edwin Antony [1,*], Krishan K. Pandey [3,*]

[1]Department of Biochemistry and Molecular Biology, School of Medicine, Saint Louis University, St. Louis, MO 63104, United States
[2]Present address: Center for Cardiovascular Research, Washington University in St. Louis, St. Louis, MO 63110, United States
[3]Department of Molecular Microbiology and Immunology, School of Medicine, Saint Louis University, St. Louis, MO 63104, United States
[4]Present address: Department of Biochemistry and Molecular Biology, University of Arkansas for Medical Sciences, Little Rock, AR 72205, United States
[5]Present address: Eppley Institute for Research in Cancer and Allied Diseases, University of Nebraska Medical Center, Omaha, NE 68198, United States

*To whom correspondence should be addressed. Email: krishan.pandey@health.slu.edu
Correspondence may also be addressed to Edwin Antony. Email: edwin.antony@health.slu.edu

Abstract

Retroviral integration is mediated by viral integrase (IN), which synapses two viral long terminal repeat DNA ends and produces a series of nucleoprotein complexes known as intasomes. While structural studies of mature intasomes have illuminated key aspects of their architecture and provided insights into the integration reaction, the sequence of events driving IN oligomerization and engagement of the viral DNA pairing remains unclear. Here, using complementary biochemical and biophysical approaches, including ensemble and single-molecule Förster resonance energy transfer, we reveal that integration progresses through a key transient intermediate that leads to the mature intasome. We demonstrate that Rous sarcoma virus intasome assembly pathway proceeds through a tetrameric intermediate where two IN dimers engage a single DNA end. This complex subsequently oligomerizes to form mature, functional octameric intasome in which two DNA ends are juxtaposed for concerted integration. These findings provide mechanistic insights into the stepwise pathway of retroviral integration and define a previously uncharacterized intermediate critical for intasome maturation, and possibly a drug target for clinically relevant retroviruses.

Graphical abstract

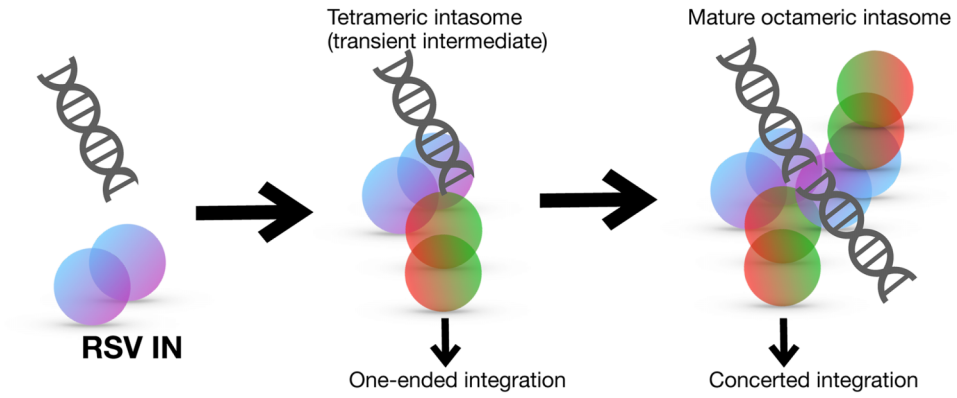

Introduction

Retrovirus integrase (IN) possesses a unique ability to insert the ends of linear viral DNA in a concerted fashion into the host genome, a step required for virus replication. Despite advances in our understanding of integration from structural studies, there is a substantial gap in deciphering the assembly mechanisms associated with these IN/viral DNA complexes, here termed intasomes. IN from Rous sarcoma virus (RSV), Human immunodeficiency virus type 1 (HIV-1), and related retroviruses share a conserved three-domain architecture composed of a catalytic core domain (CCD) that is flanked by amino (NTD) and carboxy-terminal domains (CTDs) [1–3]. The NTD adopts a three-helix bundle and contains the conserved HHCC motif that coordinates a Zn^{2+} ion [4, 5]. The

Received: September 9, 2025. **Revised:** February 17, 2026. **Accepted:** February 18, 2026
© The Author(s) 2026. Published by Oxford University Press.
This is an Open Access article distributed under the terms of the Creative Commons Attribution-NonCommercial License (https://creativecommons.org/licenses/by-nc/4.0/), which permits non-commercial re-use, distribution, and reproduction in any medium, provided the original work is properly cited. For commercial re-use, please contact reprints@oup.com for reprints and translation rights for reprints. All other permissions can be obtained through our RightsLink service via the Permissions link on the article page on our site—for further information please contact journals.permissions@oup.com.

Downloaded from https://academic.oup.com/nar/article/54/6/gkag270/8550793 by guest on 01 April 2026

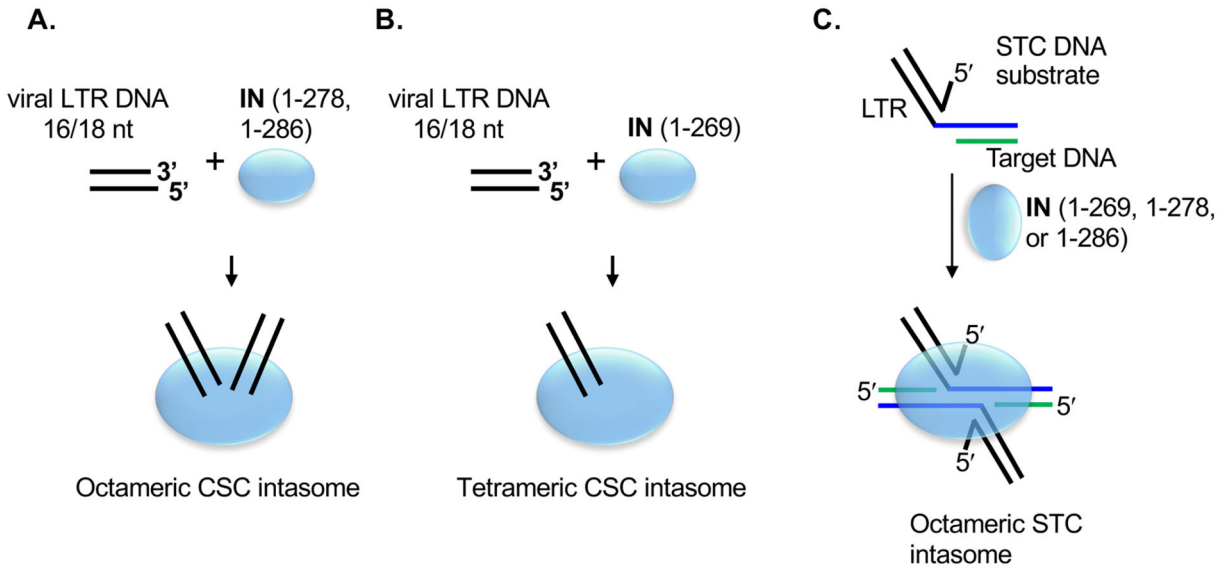

Figure 1. RSV intasome assembly showing the terminal IN–DNA complexes produced *in vitro*. (**A**) The wild-type (WT) full-length RSV IN (1–286 aa) or the IN (1–278), having an 8-aa truncation in the C-terminal tail region binds to viral LTR DNA ends, resulting in the assembly of a stable octameric CSC. (**B**). IN (1–269), having a truncation of complete 17-aa tail region, and certain missense IN mutants produce a tetrameric CSC intasome only. (**C**) STC can be assembled *in vitro* using a branched STC substrate mimicking viral DNA covalently joined to target DNA. All of RSV INs produce octameric STC intasome. Multimeric forms of IN are not shown in these schematics.

CCD is the most conserved domain among retroviruses and contains the active site comprising the DDE (Asp-Asp-Glu) motif which is responsible for catalytic activity [6, 7]. The CTD, which adopts an SH3-like fold, is the least conserved domain [8]. The CTD is proposed to be the primary factor driving formation of different oligomeric forms of nucleoprotein complexes observed with different retroviral INs [9, 10]. The structure of the flexible C-terminal tail region, which extends beyond the CTD, has not been fully resolved. The 17-aa tail region (270–286 aa) in RSV IN has a key role in defining intasome architecture [11–13].

During integration, IN binds both ends of linear viral DNA (generated by reverse-transcription) and removes two nucleotides from the 3′-termini of catalytic strand producing cleaved synaptic complex (CSC). IN within the CSC intasome binds host DNA to form the strand transfer complex (STC) and mediates the nicking of host DNA and joining of viral DNA to host DNA. In this study, intasome specifically refers to the complex formed with IN and viral DNA. In general, most intasome assemblies observed *in vitro* suggest DNA-mediated tetramerization of the predominant IN species observed in solution although the precise oligomeric states vary across retroviruses. Intasomes are composed of IN multimers ranging from four subunits for prototype foamy virus [14], human T-cell leukemia virus [15], and simian T-lymphotropic virus type 1 [16] to 8 for alpha-retrovirus RSV [17, 18] and beta-retrovirus mouse mammary tumor virus [19, 20]. Lentiviral intasomes display greater variability, containing between 4 and 16 IN subunits [21–24]. Thus, intasomes exhibit considerable structural diversity despite conserved catalytic function.

Available intasome structures represent end-products of the integration pathway; the CSC formed with IN and viral long terminal repeat (LTR) DNA and the STC formed with a branched DNA substrate mimicking viral LTR DNA covalently joined to the target DNA. We previously showed that the C-terminal tail region of RSV IN plays a critical role in determining the CSC intasome architecture (Figs 1 and 2). RSV

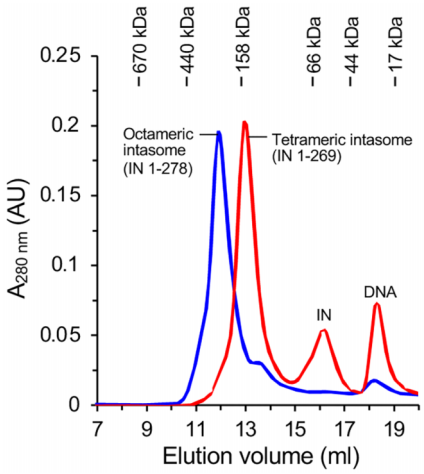

Figure 2. Differential assembly of RSV intasomes. Octameric and tetrameric intasomes are exclusively end-products formed with IN (1–278 aa) or IN (1–269 aa).

IN (1–269), lacking the tail region, predominantly forms the tetrameric intasome (Figs 1B and 2), whereas full-length RSV IN (1–286) forms the octameric intasome [11]. IN (1–278) was the most efficient in producing octameric intasomes as end-products [12] (Figs 1A and 2). Interestingly, truncations within the C-terminal tail region (270–286 aa) did not significantly affect the 3′-processing [12], strand transfer activities, and their ability to produce STC in presence of a target DNA (Fig 1C and Supplementary Fig. S1). Strand transfer and 3′-processing activity is typically measured at 37°C, while the intasome assembly is carried out at 18°C to prevent catalysis.

We previously reported that mature octameric intasome formation with IN (1–278) and IN (1–286) was preceded by a tetrameric complex [12]. We hypothesize that there are key

Downloaded from https://academic.oup.com/nar/article/54/6/gkag270/8550793 by guest on 01 April 2026

intermediates in the intasome assembly pathway with distinct IN multimers and viral DNA, which subsequently results in the binding of target DNA and integration. We proposed that RSV tetrameric intasome may be a transient precursor to the mature octameric intasome. In this study, we further establish the steps associated with formation of tetrameric intasome precursor and its conversion to mature octameric intasome. Our results show that the precursor tetrameric intasome consists of two IN dimers bound to a single DNA molecule, which subsequently oligomerizes to yield the functional mature octameric intasome. These findings provide mechanistic insight into the stepwise assembly of retroviral intasomes and identify a previously uncharacterized intermediate that is critical for integration.

Materials and methods

RSV IN expression and purification

RSV IN constructs were expressed in *Escherichia coli* BL21(DE3)pLysS (Agilent Technologies) and purified to near-homogeneity (Supplementary Fig. S2). The WT Prague A IN subunit, 286 aa in length, designated IN (1–286) was cloned in *Nde*I-*Bam*HI site of pET11a. Site-directed mutagenesis was carried out to generate truncations of C-terminal tail region and active site mutants (D64K, D121A). The DNA sequences of all IN constructs were confirmed by sequencing. For this study, RSV IN (1–278 aa) is simply referred to as RSV IN. The bacterial cells transformed with various expression IN constructs were grown in Terrific broth media at 37°C to an $A_{600\,nm}$ of 1.5 prior to induction with 0.4 mM isopropyl-thio-β-D-galactopyranoside. Cells were harvested by centrifugation following 3 h of induction at 37°C. IN was extracted by sonication in high-salt buffer (50 mM HEPES, 1 M NaCl, 1 mM TCEP, pH 7.5) and purified by two-step ion-exchange chromatography. The extracts were diluted to 500 mM NaCl and loaded on a 5 ml HiTrap SP HP column (Cytiva Life Sciences), and bound protein eluted in a linear gradient of 0–1 M NaCl [50 mM HEPES, 10 mg $MgSO_4$, 1 mM ethylenediaminetetraacetic acid (EDTA), 1 mM TCEP pH 7.5]. Top IN fractions identified by sodium dodecyl sulfate (SDS)–polyacrylamide gel electrophoresis were loaded on a 5 ml EconoFit Macro-Prep High S Column (Bio-Rad) and eluted with linear gradient of 0–1.7 M NaCl (50 mM HEPES, 10 mg $MgSO_4$, 5% glycerol, 1 mM EDTA, 1 mM TCEP, pH 7.5). Purified IN fractions were pooled and concentrated to 20–30 mg/ml using Amicon Ultra-15 centrifugal filters (30K MWCO). INs were predominantly dimeric in solution (Supplementary Fig. S3). The protein concentrations were reported as monomeric forms.

Viral DNA substrates and concerted integration assay

The concerted integration assays were performed using 3′-OH recessed oligonucleotide viral DNA substrates and RSV IN as described previously [11, 12]. Double-stranded 3′-OH recessed substrates containing RSV gain-of-function(G) U3 were generated by annealing oligonucleotides synthesized by Integrated DNA Technologies. The DNA substrates were recessed by two nucleotides on the catalytic strand and designated with "R." The oligonucleotide length denotes the non-catalytic strand. The sequences were as follows: 18R GU3 (5′-ATT GCA TAA GAC AAC A-3′ and 5′-AAT GTT GTC TTA TGC AAT-3′), 20R GU3 (5′-GTA TTG CAT AAG ACA ACA-3′ and 5′- AAT GTT GTC TTA TGC AAT AC-3′). In select experiments, the 18-nt non-transferred strand was labeled with Cy3 at 5′end. The blunt-ended substrate (18B) was generated by annealing (5′-ATT GCA TAA GAC AAC ATT-3′ and 5′-AAT GTT GTC TTA TGC AAT-3′). The bold underlined nucleotide on the catalytic strand differed between the GU3 and WT U3 sequence. The typical assay contained IN and 18R GU3 at 2 and 1 μM concentration, respectively, in 20 mM HEPES, pH 7.5, 125 mM NaCl, 10 mM $MgCl_2$, 5 mM dithiothreitol (DTT), and 10% (v/v) dimethyl sulfoxide (DMSO) in a total volume of 50 μl. After initial preincubation of the IN/DNA mixture at 14°C for 15 min, the supercoiled target DNA (300 ng pUC19) was added, and strand transfer was carried out at 37°C for 30 min. Reactions were stopped with EDTA to a final concentration of 25 mM, and samples were deproteinized with 0.5% SDS, 1 mg/ml proteinase K for 1 h at 37°C. The strand transfer products were resolved on a 1.3% agarose gels, stained with SYBR Gold (Invitrogen), and analyzed using a Typhoon 9500 Laser Scanner (GE Healthcare).

Assembly of the RSV cleaved synaptic complex

RSV CSC intasomes were assembled with IN and 18R GU3 in the presence or absence of integrase strand transfer inhibitor (INSTI) MK-2048 [11]. The intasomes were analyzed by size-exclusion chromatography (SEC) using Superdex 200 Increase (10/300) (Cytiva Life Sciences) at 4°C. The intasome assembly without INSTI was performed in 20 mM HEPES, pH 7.5, 150 mM NaCl, 50 mM $MgSO_4$, 1 M non-detergent sulfobetaine (NDSB)-201, 10% DMSO, 10% glycerol, and 1 mM tris(2-carboxyethyl)phosphine (TCEP). Intasomes were purified by SEC in 20 mM HEPES, pH 7.5, 150 mM NaCl, 50 mM $MgSO_4$, 5% glycerol, and 1 mM TCEP. The assembly reactions that contained INSTI MK-2048 were carried out in 20 mM HEPES, pH 7.5, 100 mM NaCl, 100 mM ammonium sulfate, 1 M NDSB-201, 10% DMSO, 10% glycerol, 1 mM TCEP. INSTI bound intasomes were purified by SEC in 20 mM HEPES, pH 7.5, 200 mM NaCl, 100 mM ammonium sulfate, 5% glycerol, and 1 mM TCEP. Reaction mixture typically contained 45 μM IN (as monomers), and 15 μM 3′-OH recessed oligonucleotide, and where indicated 125 μM MK-2048. MK-2048 was generously provided by Merck & Co. The samples were incubated at 18°C for 18 h unless otherwise indicated. For time-course experiments, the half-time ($t_{1/2}$) of the tetramer-to-octamer conversion was determined by non-linear fit using equation "$Y = Y_0 + (\text{Plateau-}Y_0)\ (1\text{-exp}^{-Kx})$"; where Y_0 is the initial value, plateau is the Y value at 24 h, K is the rate constant, expressed in reciprocal of X unit (time). The half-time ($t_{1/2}$) was computed as ln[2]/K. Individual data points representing independent experiments ($n \geq 3$ per time point) are shown as a scatter plot (Supplementary Fig. S4). All statistical analyses were carried out in Graph Pad Prism 10.

For functional characterization of intasome oligomerization, octameric and tetrameric intasomes were purified by SEC from assembly reactions incubated for 24 and 1 h, respectively, in absence of INSTI (Fig. 3). Equimolar concentrations of two intasome fractions each were used for strand transfer at 37°C for 10 min with 300 ng target DNA (pUC19). The

Downloaded from https://academic.oup.com/nar/article/54/6/gkag270/8550793 by guest on 01 April 2026

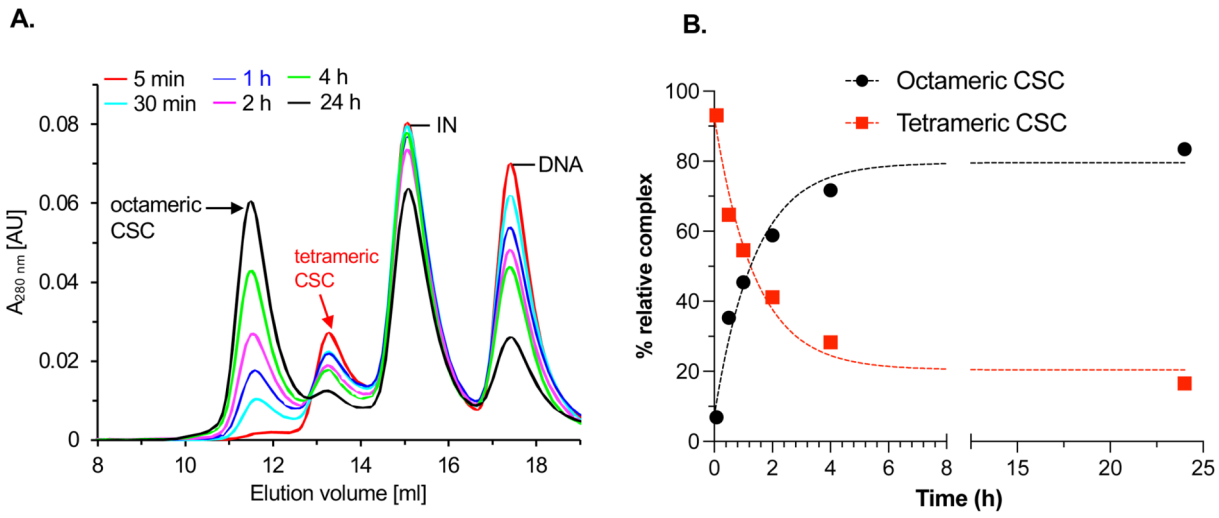

Figure 3. Transient RSV tetrameric CSC intasome is rapidly converted to octameric CSC intasome in absence of INSTI. (**A**) SEC profiles of a time course of CSC intasome assembly with RSV IN (1–278) without INSTI. Tetrameric CSC intasomes are formed early and rapidly converted to octameric CSC intasomes. (**B**) Quantitation of relative percentage of intasomes. Dotted lines indicate non-linear fit ($t_{1/2}$ = 0.96 ± 0.3 h).

reactions were deproteinized and analyzed on 1.3% agarose gel (Supplementary Fig. S5).

Native mass spectrometry

The purified IN and intasomes were analyzed by native mass spectrometry (MS) to determine their mass and stoichiometry (Supplementary Fig. S6). The intasomes were assembled and purified as described earlier in presence of MK-2048 under conditions to maximize the production of octamer or tetrameric complex. Following purification by SEC in buffer devoid of glycerol, intasome samples were buffer exchanged into 200 mM ammonium acetate using Micro Bio-Spin 6 columns (Bio-Rad). For native MS analysis, sample was loaded into a commercial borosilicate emitter (ES380, Thermo Scientific, Hudson, NH, USA) using a gel loader tip and was briefly centrifuged (2–3 s) to move the fluid to tip of the emitter. The emitter was then mounted onto the ESI source of a Thermo Exactive Plus EMR Orbitrap mass spectrometer (Thermo Scientific, Waltham, MA, USA). MS data were collected in the positive ion mode over a m/z range of 1000–9000 with a source voltage of 0.9–1.2 kV and capillary temperature of 150°C. Data were processed using Unidec software. Native MS was carried out at WUChem Biomedical Mass Spectrometry Facility located at Washington University in St. Louis, MO.

Mass photometry

The SEC-purified fractions containing tetrameric and octameric fractions were analyzed by a TwoMP instrument (Refeyn Inc) as described [25]. Briefly, the purified complexes were diluted in 20 mM HEPES, 100 mM NaCl, 200 mM ammonium sulfate, 1 mM TCEP, pH 7.5 and immediately applied on a clean slide for light scattering measurements at a final concentration of 5 nM. Molecular weight standards were resuspended in matching buffer and used to calibrate and convert the particle-image contrast due to scattered light into MW units. Standards included β-amylase (three species of 56, 112, and 224 kDa, respectively) and thyroglobulin (single species of 667 kDa).

Steady-state fluorescence (bulk-FRET)

RSV IN intasomes were assembled as described earlier using viral LTR DNA internally labeled at position 9 with Cy3 (iCy3-18R GU3; 5′-AAT GTT GTC /iCy3/TTA TGC AAT-3′) or Cy5 and (iCy5-18R GU3; 5′-AAT GTT GTC/iCy5/TTA TGC AAT-3′) on the non-transferred strand and annealed with complementary transferred strand (5′-ATT GCA TAA GAC AAC A-3′). Equimolar quantities (7.5 μM each) of iCy3 18R-GU3 (donor)- and iCy5 18R-GU3 (acceptor)-labeled annealed 18R GU3 were used in the assembly mixture. Labeling at position 9 was not expected to affect IN binding or intasome assembly, as determined from the IN–DNA interactions in cryo-EM structures [18, 26]. The distance between 9th nucleotide on two DNA ends within the CSC intasome is 39 Å, which is appropriate for Förster resonance energy transfer (FRET) analysis [18, 26]. The complexes were assembled under conditions suitable to allow purification of tetrameric as well as octameric intasomes from the same sample. Intasome assembly and concerted integration was not affected by internal fluorophore labeling of viral LTR DNA. Octameric and tetrameric intasomes, purified by SEC, were analyzed using a Fluoromax-3 (Jobin Yvon, Inc., Edison, NJ) spectrofluorometer at 14°C with a temperature-regulated cell holder. The samples were excited with 550 nm (donor excitation), and emission spectra were collected from 555 to 720 nm for quenching of Cy3 (peak at 565 nm) and sensitized emission of Cy5 (peak at 668 nm). All spectra were corrected for buffer and instrument.

Single-molecule FRET

The SEC purified fractions containing tetrameric or octameric fractions were analyzed by single-molecule FRET (smFRET)-TIRFm (total internal reflection fluorescence microscopy). The complexes were assembled with equimolar ratio of iCy3 18R-GU3 (donor)- and iCy5 18R-GU3 (acceptor)-labeled 18R GU3 (7.5 μM each) with RSV IN (45 μM). The tetrameric and octameric intasomes were purified using SEC and immediately analyzed by smFRET. Intasome complexes were loaded onto pre-cleaned coverslip-chambers. The complexes were

Downloaded from https://academic.oup.com/nar/article/54/6/gkag270/8550793 by guest on 01 April 2026

allowed to settle down passively. Excess molecules were washed off using binding buffer (20 mM HEPES, pH 7.5, 200 mM NaCl, 100 mM ammonium sulfate, and 1 mM TCEP). Single molecule TIRF imaging was performed in the same buffer supplemented with oxygen scavenging system and Trolox using an inverted, objective based total-internal-reflection fluorescence microscope (TIR-FM; IX71 Olympus). Samples were excited with a 532nm laser or 637nm laser to excite the donor or the acceptor, respectively. Donor fluorescence (green traces) and energy-transferred acceptor traces (red) were collected at the rate of 100 ms frame time using an EM-CCD (iXon Ultra DU-897U-CS0). The data analysis was carried out as described earlier [27].

To analyze the freely diffusing intasomes in solution, sm-FRET data were collected on an EI-FLEX bench-top microscope (Exciting Instruments Ltd, Sheffield, UK) as described [28] with minor modifications. The intasomes were assembled using equimolar iCy3 and iCy5 18R GU3 with or without INSTI MK-2048 and purified by SEC as earlier. Before measurement on EI-FLEX, respective SEC buffers were photo irradiated using 100W LED bulb for 3 days in cold room (4°C). Buffers were supplemented with 1 mM TCEP and 0.1 mg/ml photo-irradiated bovine serum albumin for intasome dilutions just before the measurement. Octamer and tetramer intasome were diluted to 10 pM on ice. A 100 µl sample droplet was placed onto a no.1 thickness coverslip and excited with alternating 520 nm (0.22 mW) and 638 nm (0.15 mW) lasers, respectively. Lasers were sequentially turned ON for 45 µs for each measurement and separated by a dark period of 5 µs for a total of 30 min of acquisition at room temperature (21°C). Fluorescence emission photons from freely diffusing molecules were collected using an Olympus 60× (1.2 N.A.) water-immersion objective, focused onto a 20 µm pinhole. After passing through the pinhole, the photons were split using a 640 nm long-pass filter, cleaned up using 572 and 680 nm band-pass filters, and focused onto respective avalanche photodiodes. The photon arrival times, and respective detector were saved in HDF5 data format for offline analysis. Several measurements were recorded with freshly diluted samples for each intasome populations. The data were analyzed in Anaconda environment (2.6.6) with Jupyter notebooks, using FRETBursts Python package 0.7.1 [29]. FRET values of single-molecule bursts of photon emissions were exported in Excel sheets then plotted as FRET histograms in GraphPad Prism 10.

Stopped-flow analysis of IN–DNA interactions

To monitor the initial interactions between IN and DNA leading to the assembly of CSC, we performed stop flow experiments to monitor the IN–DNA (iCy3-18R GU3) dynamics using an Applied Photophysics SX20 (UK) instrument in reaction buffer containing 20 mM HEPES, pH 7.5, 125 mM NaCl, 10 mM $MgCl_2$, 10% DMSO (v/v), and 5 mM DTT. The change in photoisomerization-induced fluorescence enhancement of Cy3 was measured upon binding to IN. 100 nM iCy3-18RGU3 DNA and varying amount of RSV IN (20–300 nM) were rapidly mixed and monitored by exciting the samples at 530 nm, and emission was measured using a 555 nm cut-off filter. Protein and DNA concentrations denoted here are pre-mixing conditions, which are reduced to half after mixing the DNA and IN to provide final post-mixing concentrations. The protein-induced fluorescence enhancement was monitored as IN binding enhanced the Cy3 fluorescence signal and fitted using a single exponential equation and the rate of change was plotted as a function of IN concentration (Supplementary Fig. S7). The association constant (k_{ON}) and dissociation rate constant (k_{OFF}) were determined to be 5.6×10^8 $M^{-1}s^{-1}$ and 8.86 s^{-1}, respectively, by fitting the data to a linear equation. As expected, IN binds tightly to viral DNA with a dissociation constant of ∼15.8 nM.

Results

Characterization of a novel assembly intermediate in the RSV integration pathway

Intasome structures from several retroviruses have revealed the architecture of their end-products in the concerted integration pathway. However, the pathways leading to formation of mature intasomes from IN and DNA are not well understood. Therefore, in this study, we investigated the assembly pathway using RSV IN and viral DNA, in the absence/presence of INSTI MK-2048, as a function of time. MK-2048, like other INSTIs is a strand transfer inhibitor which prevents the target DNA binding to IN-viral DNA complexes thus preventing integration [30, 31]. In absence of viral DNA, IN remains predominantly dimeric (Supplementary Fig. S3).

In absence of INSTI, a tetrameric intasome is formed first and gradually converted into mature octameric intasomes (Fig. 3 and Supplementary Fig. S4A). The $t_{1/2}$ for the tetramer to octamer transition is 0.96 ± 0.3 h. In the presence of MK-2048 during assembly, the tetrameric intasome accumulates rapidly with peak yield between 30 min and 1 h and subsequently decreases with time with concomitant increase in octameric intasome assembly (Fig. 4 and Supplementary Fig. S4B). The $t_{1/2}$ for the tetramer to octamer transition is 2.94 ± 0.5 h. Notably, INSTI was not included during intasome purification by SEC irrespective of presence or absence of INSTI during the intasome assembly. The purified octameric and tetrameric intasomes assembled for 24 and 1 h respectively were used directly at equimolar concentration to assess their ability for strand transfer. (Supplementary Fig. S5). The results showed higher concerted products with octameric intasomes confirming that it is primed to binding target DNA and concerted integration. Intasome assembly with the blunt DNA substrate (18B) show similar kinetics though the overall yield of intasome is much lower compared to pre-processed substrates (Supplementary Fig. S8). The length of viral DNA substrate used in intasome assembly was empirically determined. 18R yielded most robust yield and stable complexes suitable for structure determination [18]. Intasome produced with longer (≥ 20R) viral DNA substrates had lower solubility and yield (data not shown). As expected, the IN catalytic mutants D64K and D121A defective for strand transfer [32] (Supplementary Fig. S3D) did not produce either tetrameric intermediate or mature octameric intasomes (Supplementary Fig. S9). These data confirm earlier reports using HIV-1 IN [31] and RSV IN [11] that INSTI is not required for the assembly of intasomes. Rather, INSTI such as MK-2048 traps and stabilizes the intasomes in solution resulting in their higher yield.

Downloaded from https://academic.oup.com/nar/article/54/6/gkag270/8550793 by guest on 01 April 2026

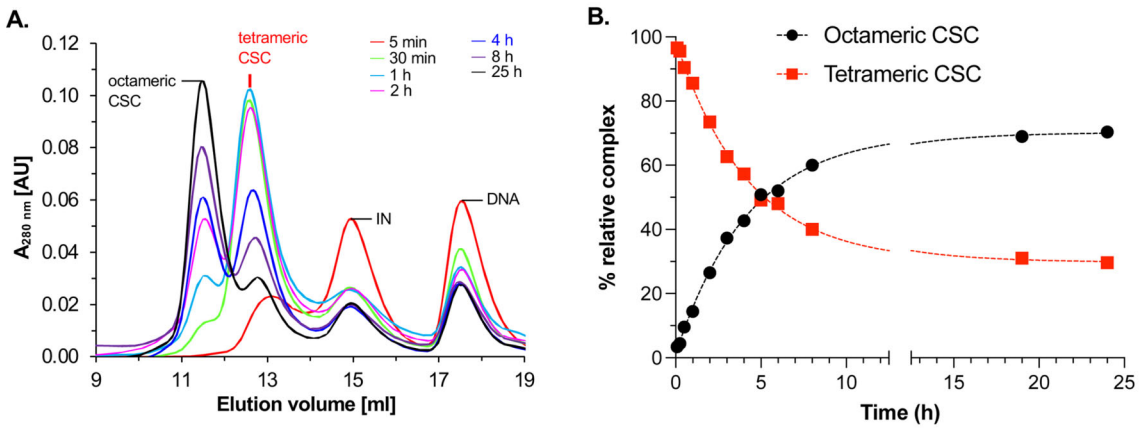

Figure 4. RSV tetrameric CSC intasome is an assembly intermediate for the mature octameric CSC intasome *in vitro*. (**A**) SEC profiles for a time course of CSC intasome assembly with RSV IN (1–278) in presence of INSTI MK-2048 at 18°C. Selected assembly time points are shown for clarity. Tetrameric CSC intasomes are formed early in the assembly pathway that are gradually converted to octameric CSC intasomes. (**B**) Relative percentage yield of intasome is plotted at all assembly time points. Dotted lines indicate non-linear fit ($t_{1/2}$ = 2.94 ± 0.5 h).

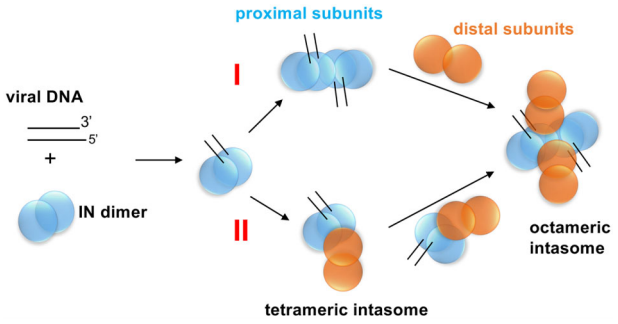

Figure 5. Potential assembly pathways of RSV intasome. Proximal and distal IN protomers are shown in blue and orange, respectively.

Pathway choice for oligomerization routes through a single DNA-bound tetrameric intasome intermediate

In the RSV integration pathway, DNA binding drives formation of the tetrameric intasome which then matures into the octameric form. Cryo-EM studies of the octameric RSV intasome revealed two DNA ends bound to opposing IN dimers [18]. We have established that a DNA-bound tetrameric intasome is a precursor to the mature octamer. The structure of tetrameric intasome precursor is not available and the mechanistic details of how it is assembled in the presence of DNA remains poorly understood. To parse this mechanism further, we started out with two possible pathways for the assembly of the RSV intasome (Fig. 5).

In the first pathway, two DNA -bound IN dimers (that form the proximal subunits in the final octamer) oligomerize to form an IN tetramer complex. In this scenario, both DNA fragments are sequestered, and the subsequent steps involve engagement of the distal IN dimers leading to formation of the octameric intasome. The second pathway posits an intermediate where one DNA-bound IN dimer oligomerizes with a distal IN molecule generating a tetramer containing a single DNA which then rearranges to produce mature octameric intasome (Fig. 5). The key difference in the second pathway is that the two DNA fragments encounter each other only within the context of the octamer. We observed that DNA binding to RSV IN is rapid in stopped flow experiments (Supplementary Fig. S7). In these experiments, a Cy3 labeled DNA was used and the change in Cy3 fluorescence upon binding to IN was monitored. The rate of DNA binding is much faster than the oligomerization observed in time course experiments (Figs 3 and 4). Therefore, with respect to pathway choice, initial IN–DNA interactions occur rapidly.

To experimentally distinguish between two pathway choices towards formation of the terminal octameric intasome, we used FRET to test the binding of two fluorescently labeled LTR DNAs with either Cy3 or Cy5. Equal quantities of both labeled DNAs were mixed with IN to assemble the intasomes and both the tetrameric and octameric intasome were separated by SEC (Fig. 6A). Assembly of two DNA fragments within the fractions containing tetramer and/or the octamer intasomes should give rise to a high FRET signal.

The efficiency of separation of the two species was further confirmed using mass photometry. The octameric intasome fraction displayed a predominant ∼270 kDa peak that corresponds to the octamer along with smaller ∼60 and ∼130 kDa peaks that correspond to the dimeric and tetrameric species, respectively (Fig. 6B and C). The tetrameric intasome fraction displayed two major species that correspond to the ∼60 kDa dimer and ∼130 kDa tetramer, respectively, along with a very minor species for the octamer. Native MS of tetrameric intasome displayed a measured mass of 134.2 kDa consistent with IN tetramer bound to a single DNA substrate (Supplementary Fig. S6B). Octameric intasome displayed a mass of 262.4 kDa (Supplementary Fig. S6C) consistent with a complex comprising four IN dimers and two molecules of 18R DNA as observed in the cryo-EM structure [18].

The tetrameric and octameric intasome fractions carrying the labeled DNA were subsequently analyzed for changes in Cy5 fluorescence signal by exciting the Cy3 donor. Fluorescence emission scanning of both samples after excitation of the Cy3 shows a robust increase in the Cy5 signal for the octameric complex compared to the tetrameric complex (Fig. 6D). This suggests that two DNA molecules in the octameric complex are bound and aligned as observed in the cryoEM structure [18] and positioned to generate robust FRET. In contrast, the lack of a FRET-induced Cy5 signal for the tetrameric sample suggests that this complex is composed of one DNA-bound IN dimer and a dimer of the proximal subunits not bound to DNA (pathway II; Fig. 5).

Downloaded from https://academic.oup.com/nar/article/54/6/gkag270/8550793 by guest on 01 April 2026

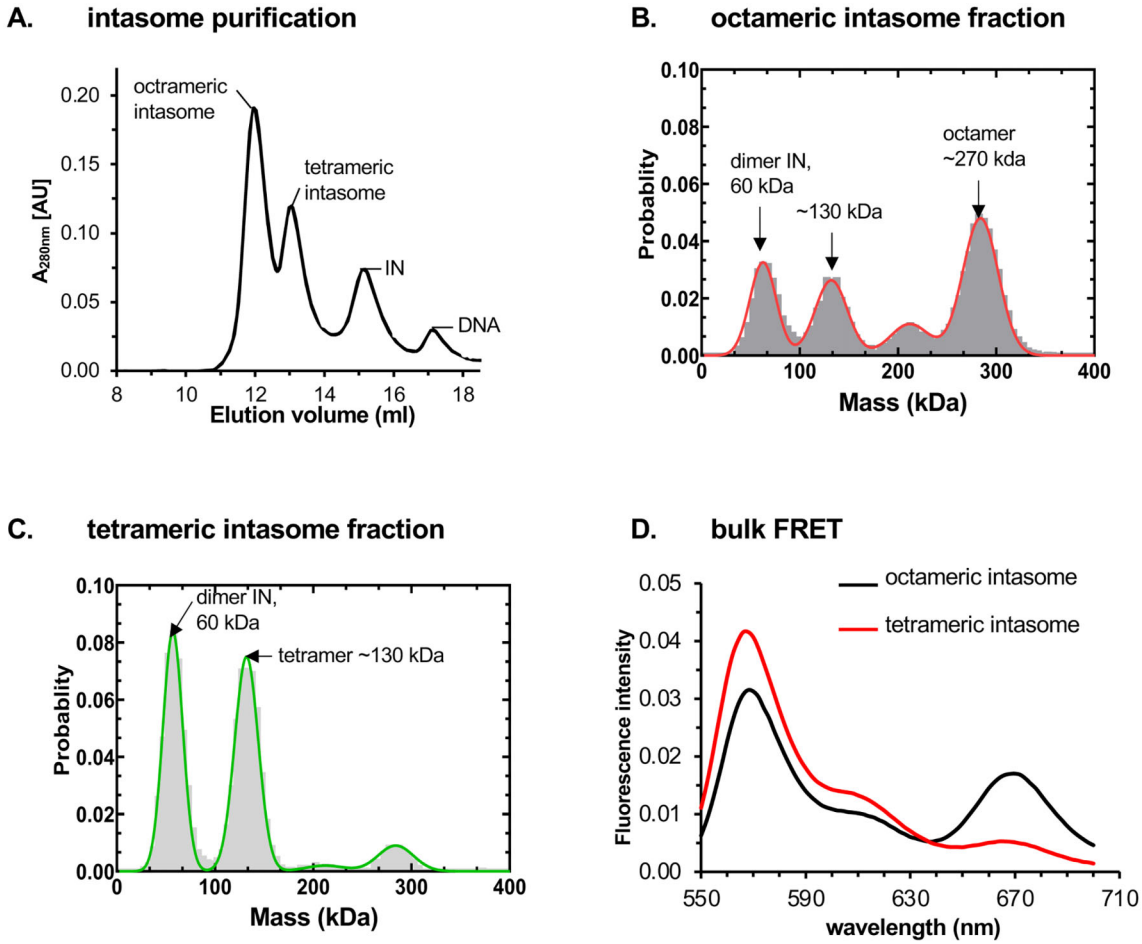

Figure 6. Characterization of transient tetrameric and mature octameric intasomes assembled with RSV IN.(**A**) The SEC purification profile of CSC intasomes assembled with IN 1–278 and Cy3/Cy5 labeled 18R GU3 LTR DNA in presence of INSTI MK-2048. The top fractions of octameric and tetrameric intasome were analyzed by mass-photometer (B and C, respectively) and bulk FRET (D). (**B**, **C**) Octameric and tetrameric fractions showed molar mass predominantly of ∼270 and ∼130 kDa, respectively. Dimeric IN (∼60 kDa) was also observed probably due to complex dissociation during analysis. (**D**) Bulk-FRET of octameric and tetrameric intasomes. Normalized FRET profiles show that FRET was observed predominantly in octameric intasomes only.

Single-molecule FRET confirms the one-DNA-bound tetrameric intasome intermediate

The ensemble FRET studies suggests that the transient tetrameric IN–DNA complex intermediate is likely engaged to only one DNA molecule. However, the lack of FRET-induced increase in Cy5 fluorescence could also be explained by the engagement of two DNA molecules in the tetramer but bound in an orientation that is not conducive for FRET. To rule out this possibility, we used smFRET to directly visualize the complexes and individually quantitate the co-localization of the Cy3 and Cy5 fluorescence signals. The tetrameric and octameric intasomes that were formed with Cy3/Cy5-labeled DNA in presence of INSTI MK-2048 and separated by SEC fractionation were passively coated onto cover slips and imaged using smFRET-TIRFm. We observed dynamic smFRET in only the octameric intasome fractions showing distinct transitions from high to low FRET states (Fig. 7A). The majority of intasome particles containing Cy3 and Cy5 labeled DNA showed FRET (Fig. 7B). In contrast, the majority of tetrameric intasome particles had either Cy3 or Cy5 labeled DNA individually and hence no FRET was observed (Fig. 7B). These results point to pathway II being the most plausible pathway in RSV intasome assembly. These are the first of kind single molecule studies of retroviral intasome assembly systems that characterize the intermediate IN–DNA complexes.

To further quantitate these DNA binding events, we performed smFRET measurements using an EI-FLEX single molecule fluorescence spectrometer which utilizes alternating-laser excitation [33] to specifically sort molecules containing both donor and acceptor fluorophores. SEC purified octameric and tetrameric intasomes were diluted to 10 pM and FRET measured in-solution. The SEC purified intasomes remain stable during the measurement as evident by their re-chromatography (Supplementary Fig. S10). Lower yield of tetrameric intasome (in absence of INSTI) and its tendency to rapidly convert to mature octameric intasome did not allow us to determine its stability.

The octameric intasome had significantly higher counts showing high FRET efficiency (Fig. 8A) compared to the tetrameric intasome (Fig. 8B). These data confirm that octameric intasome has two DNA ends sequestered, while tetrameric complex has just one DNA end, thus making pathway II (Fig. 5) as the predominant route for intasome assembly. Similar results were obtained when the intasomes were assembled in presence of INSTI MK-2048 (Fig. 8C and D). Tetrameric intasome formed with RSV IN (1–269) did not

Downloaded from https://academic.oup.com/nar/article/54/6/gkag270/8550793 by guest on 01 April 2026

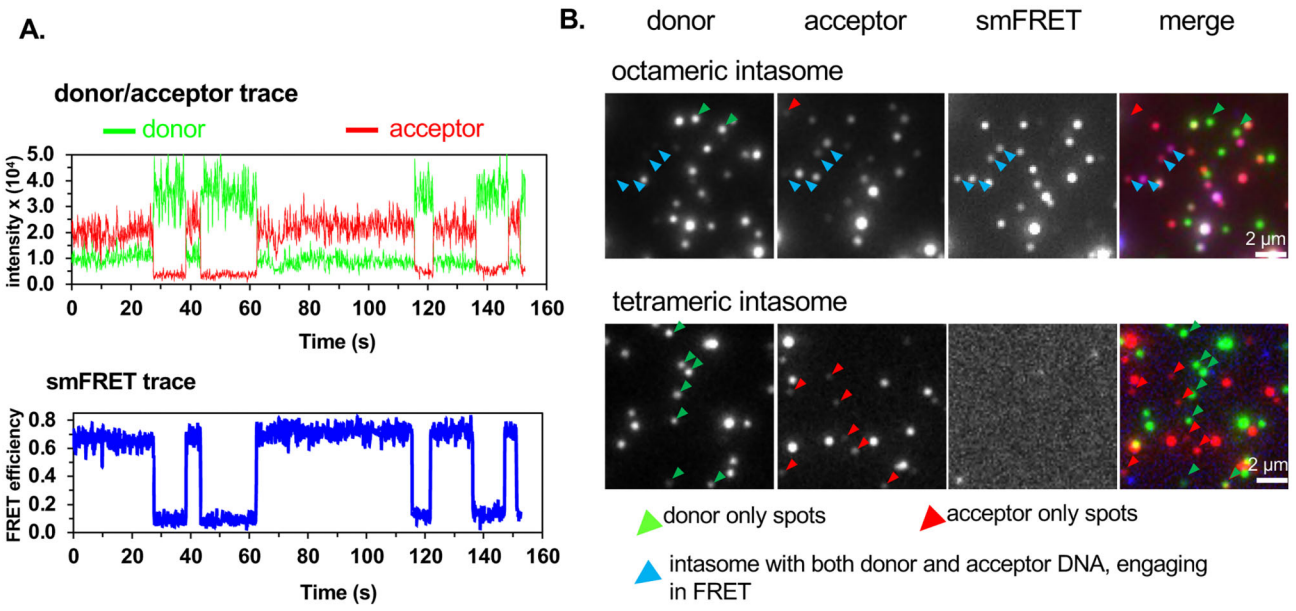

Figure 7. Visualization of intasome complexes by smFRET. (**A**) Traces of smFRET of the octameric intasome showing dynamic FRET; the fluorescence intensity from donor (Cy3) is shown in green and acceptor (Cy5) in red while the FRET signal is shown in blue. ON/OFF smFRET due to release/recapture of DNA molecules. (**B**) Snapshot of the single intasome particles in TIRF. The donor only and acceptor only spots are shown in green and red, respectively. The spots labeled with blue arrow contain both the donor and acceptor and show FRET. Please note that not all such particles are labeled.

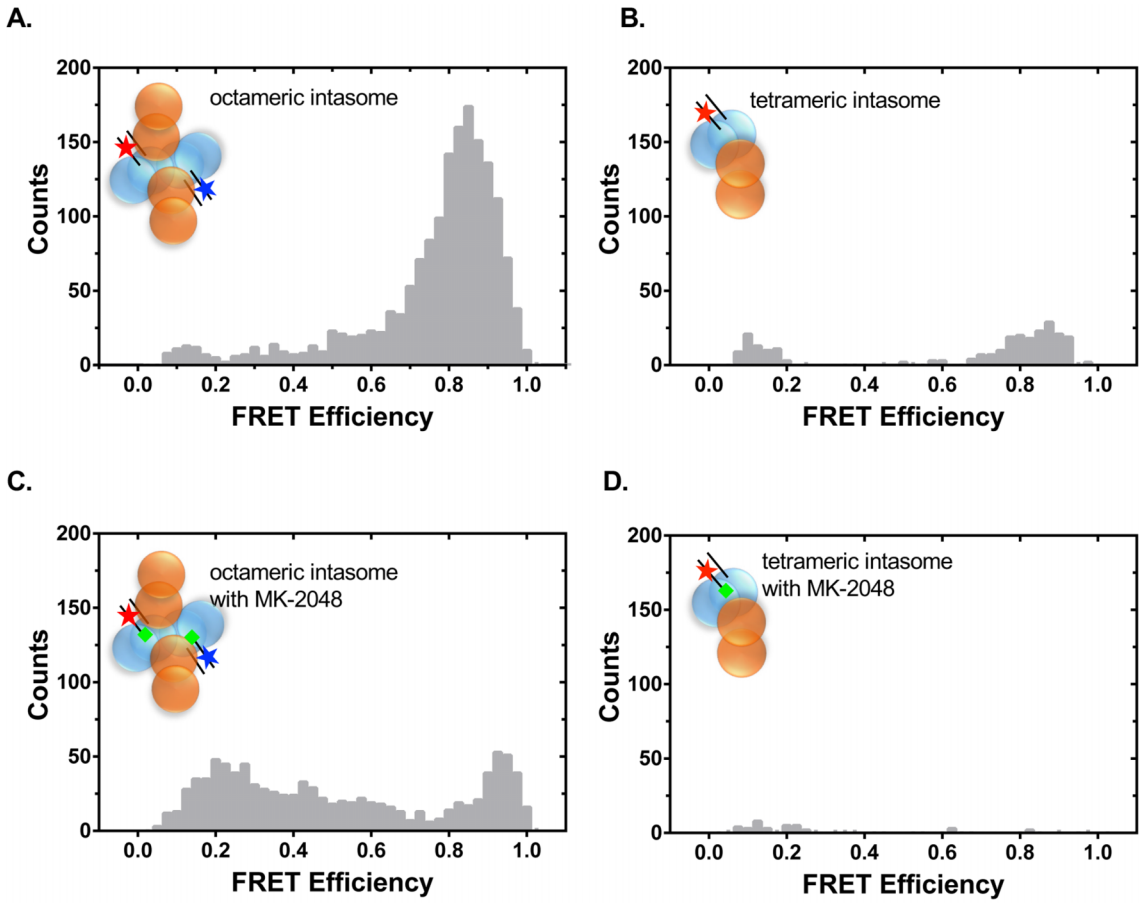

Figure 8. Confocal sm-FRET analysis of RSV intasomes using EI-FLEX. SEC purified intasomes were analyzed (10 pM) by EI-FLEX and number of counts showing FRET was plotted. The intasomes were assembled using equimolar concentration of iCy3 and iCy5 labeled 18RGU3 DNA. The fluorophores are indicated in red and blue. (**A**) Octameric intasome without drug. (**B**) Tetrameric intasome without drug. (**C**) Octameric intasome formed in the presence of INSTI MK-2048. (**D**) Tetrameric intasome in the presence of INSTI MK-2048. INSTI MK-2048 is shown in green. The FRET was observed predominantly in octameric intasomes only.

Downloaded from https://academic.oup.com/nar/article/54/6/gkag270/8550793 by guest on 01 April 2026

display FRET in a similar experiment (data not shown). It reinforces the conclusion that INSTI do not affect the intasome assembly, rather trap the intasomes in an inactive state thus preventing target DNA binding [31, 34, 35].

Discussion

Understanding the assembly mechanisms of retrovirus intasomes by IN multimers is necessary to elucidate the pathways for viral DNA integration. The structure of different retrovirus intasomes has revealed remarkable architectural diversities besides conserved structural features and catalytic mechanisms. Generally, most intasome assemblies observed *in vitro* suggest DNA-mediated tetramerization of the predominant IN species in solution. It has been difficult to obtain homogeneous intasome populations with HIV-1 or HIV-2 IN primarily due to their poor solubility and tendency to form polymeric intasome complexes instead of homogeneous uniform species of complexes produced by RSV IN under our optimized solution conditions (Fig. 2). Here, we provide evidence that assembly of the mature RSV octameric intasome *in vitro* occurs via a precursor tetrameric intermediate (Fig. 1). The ability of RSV IN to assemble the catalytically active octameric intasome from its tetrameric precursor is unique among studied retroviral systems. Whether a transient intermediate en route to mature HIV-1 intasome exists is unknown and difficult to study due to heterogeneous intasome assembly [22, 24].

We determined the structures of the RSV octameric intasome (four IN dimers and two viral DNA molecules) [18] and STC formed with a branched DNA substrate [26] by single particle cryo-EM. These structures as well as other retroviral intasome structures show that the two DNA ends are synapsed by opposing IN proximal subunits providing the catalytic actives sites and with their NTD ends swapped across the DNA-binding interface. The tetrameric intasome by virtue of being a transient precursor to mature octameric intasome has been refractory to structural studies by cryo-EM. Hence, in this study, we utilized various in-solution approaches to define the RSV intasome assembly pathway (Fig. 5).

Our data support pathway II to be the predominant route for assembly of mature octameric intasome. We provide several lines of evidence to show that tetrameric intermediate contains IN tetramer bound to single viral DNA including time dependent conversion tetramer to octamer, native MS, bulk FRET and sm-FRET. A FRET signal is only observed for the octameric intasomes suggesting that two DNA molecules are bound with their fluorophore labeled ends juxtaposed in proximity. The smFRET data further confirm that transient tetrameric intasomes contain only one DNA molecule. Therefore, no FRET signal is observed. Native MS provides additional line of evidence to determine the stoichiometry of intasomes. Our proposed model suggests that two of the tetrameric complexes undergo rearrangement to produce mature a octameric intasome. A significant rearrangement is needed to synapse two tetrameric complexes in a pathway leading to formation of mature octameric intasomes as it requires multiple cross subunits interactions between two proximal IN subunits and two DNA ends [18, 26]. Adding INSTI MK-2048 during the intasome assembly enabled us to monitor the progress of mature octameric intasome assembly from its precursor. Formation of tetramer seems to be faster than its conversion to mature octameric intasome. Within 30 min, the tetramer yield was maximum while its conversion to octamer was much slower process with gradual increase in its yield up to ∼18 h (Fig. 4). INSTI allows the accumulation of trapped intasomes. INSTI binding to the tetrameric intasome slowed its conversion to mature octameric intasome as evident from $t_{1/2}$ of 2.94 ± 0.5 h compared to 0.96 ± 0.3 h in absence of INSTI. INSTI binding to intasome delays and inhibit the formation of STC [3, 34]. In the absence of INSTI the conversion of tetrameric to octameric intasome is faster; however, the yield was lower presumably due to their lower stability. Similar kinetics are observed for intasome assembly using blunt -DNA substrate; however, the yield of complexes was minimal (Supplementary Fig. S8). It is well reported in literature that strand transfer using blunt-ended substrate is delayed due to additional step of 3′-processing required [12, 36, 37]. In our studies, intasome assembly was carried out at 18°C to prevent catalysis. RSV IN active site mutations (D64K or D121A) abolished the assembly of both the tetrameric intermediate and mature octameric intasome complexes (Supplementary Fig. S9). Consistent with their inability to assemble intasomes, these mutants were defective for concerted integration as well (Supplementary Fig. S3D). The tetrameric complex in pathway II is ideally suited to produce circular half-site products *in vitro* in which only one end of viral DNA integrates into the target DNA. RSV IN (49–286), which lacks the NTD and hence unable to provide DNA-binding interface to synapse opposing IN–DNA complex to produce CSC. However, it is still able to carry out single-ended integration event producing circular half site products [38]. This model also explains higher yield of circular half-site products at early time points in concerted integration assays [39]. On the other hand, concerted integration requires insertion of two viral DNA ends into target DNA [36, 40]. Sequential joining of two viral DNA ends to yield the concerted integration products was noted in HIV-1 integration pathway *in vitro* [41]. Purified mature RSV octameric intasome was better primed to produce concerted products in presence of a supercoiled target DNA compared to tetrameric intasome (Supplementary Fig. S5). Under identical assembly conditions without DNA in solution, the RSV IN remains dimeric (Supplementary Fig. S3) suggesting that the tetramer formed in pathway II is assembled only after initial IN dimer-DNA assembly rather DNA binding to a tetrameric IN. Whether the tetrameric intermediate exists *in vivo* is unknown. Due to very low quantities of pre-integration complexes (PICs) in infected cells, it has been technically not feasible to determine oligomeric state or structure of PICs. Time-dependent assays [42] have shown that processing occurs in cytosol before IN–DNA complex encounters cellular host DNA for strand transfer. Hence the CSC intasomes mentioned in this study mimics the IN-processed DNA complexes in cytosol.

In conclusion, in this study, we characterized a novel intermediate in the retroviral integration pathway. These findings establish a stepwise assembly model in which the RSV octameric intasome is formed through single-DNA-bound tetramers *in vitro*. Further studies are needed to ascertain whether an analogous pathway is present in HIV-1 and similar retroviruses. The approaches and assays described in this study may be useful in for dissecting intasome assembly pathways and screening for IN inhibitors.

Downloaded from https://academic.oup.com/nar/article/54/6/gkag270/8550793 by guest on 01 April 2026

Acknowledgements

We would like to thank Drs Henry Rohrs and Nuwani Weerasinghe (Washington University in St. Louis) for their help in native MS carried out at WUChem Biomedical Mass Spectrometry Facility.

Author contributions: Rahul Chadda (Formal analysis [supporting], Investigation [equal], Methodology [supporting], Visualization [supporting]), Sibes Bera (Formal analysis [supporting], Investigation [equal], Visualization [supporting]), Mohamed Ghoneim (Formal analysis [supporting], Investigation [equal], Visualization [supporting]), Tamara De Melo (Investigation [supporting]), Duane P. Grandgenett (Formal analysis [supporting], Writing—review & editing [supporting]), Edwin Antony (Conceptualization [lead], Formal analysis [supporting], Funding acquisition [lead], Investigation [supporting], Writing—review & editing [lead]), and Krishan Pandey (Conceptualization [lead], Formal analysis [lead], Funding acquisition [lead], Investigation [lead], Project administration [lead], Supervision [lead], Validation [lead], Visualization [lead], Writing—original draft [lead]).

Supplementary data

Supplementary data is available at NAR online.

Conflict of interest

None declared.

Funding

This work was supported in part by the National Institute of Allergy and Infectious Diseases (NIAID) of National Institutes of Health (NIH) AI165081 and AI175583 to K.K.P., and National Institute of General Medical Sciences GM149320 to E.A. This work was also supported partially by Saint Louis University President Research Fund (K.K.P.). E.A. would also like to acknowledge generous financial support from the Doisy Research Fund of the Edward A. Doisy Department of Biochemistry and Molecular Biology at Saint Louis University School of Medicine. The content is solely the responsibility of the authors and does not necessarily represent the official views of the National Institutes of Health. Funding to pay the Open Access publication charges for this article was provided by NIH (AI175583).

Data availability

All data needed to evaluate the conclusions in the paper are present in the paper or the supplementary materials.

References

1. Jaskolski M, Alexandratos JN, Bujacz G *et al.* Piecing together the structure of retroviral integrase, an important target in AIDS therapy. *FEBS J* 2009;276:2926–46. https://doi.org/10.1111/j.1742-4658.2009.07009.x
2. Khan E, Mack JP, Katz RA *et al.* Retroviral integrase domains: DNA binding and the recognition of LTR sequences. *Nucl Acids Res* 1991;19:851–60. https://doi.org/10.1093/nar/19.4.851
3. Engelman A, Cherepanov P. Retroviral integrase structure and DNA recombination mechanism. *Microbiol Spectr* 2014;2:1–22. https://doi.org/10.1128/microbiolspec.MDNA3-0024-2014
4. Burke CJ, Sanyal G, Bruner MW *et al.* Structural implications of spectroscopic characterization of a putative zinc finger peptide from HIV-1 integrase. *J Biol Chem* 1992;267:9639–44. https://doi.org/10.1016/S0021-9258(19)50138-7
5. Cai M, Zheng R, Caffrey M *et al.* Solution structure of the N-terminal zinc binding domain of HIV-1 integrase. *Nat Struct Mol Biol* 1997;4:567–77. https://doi.org/10.1038/nsb0797-567
6. Engelman A, Craigie R. Identification of conserved amino acid residues critical for human immunodeficiency virus type 1 integrase function *in vitro*. *J Virol* 1992;66:6361–9. https://doi.org/10.1128/jvi.66.11.6361-6369.1992
7. Vink C, Oude Groeneger AM, Plasterk RH. Identification of the catalytic and DNA-binding region of the human immunodeficiency virus type I integrase protein. *Nucl Acids Res* 1993;21:1419–25. https://doi.org/10.1093/nar/21.6.1419
8. Eijkelenboom AP, Lutzke RA, Boelens R *et al.* The DNA-binding domain of HIV-1 integrase has an SH3-like fold. *Nat Struct Mol Biol* 1995;2:807–10. https://doi.org/10.1038/nsb0995-807
9. Jenkins TM, Engelman A, Ghirlando R *et al.* A soluble active mutant of HIV-1 integrase: involvement of both the core and carboxyl-terminal domains in multimerization. *J Biol Chem* 1996;271:7712–8. https://doi.org/10.1074/jbc.271.13.7712
10. Engelman A, Hickman AB, Craigie R. The core and carboxyl-terminal domains of the integrase protein of human immunodeficiency virus type 1 each contribute to nonspecific DNA binding. *J Virol* 1994;68:5911–7. https://doi.org/10.1128/jvi.68.9.5911-5917.1994
11. Pandey KK, Bera S, Korolev S *et al.* Rous sarcoma virus synaptic complex capable of concerted integration is kinetically trapped by human immunodeficiency virus integrase strand transfer inhibitors. *J Biol Chem* 2014;289:19648–58. https://doi.org/10.1074/jbc.M114.573311
12. Pandey KK, Bera S, Shi K *et al.* A C-terminal "tail" region in the Rous Sarcoma Virus integrase provides high plasticity of functional integrase oligomerization during intasome assembly. *J Biol Chem* 2017;292:5018–30. https://doi.org/10.1074/jbc.M116.773382
13. Bera S, Pandey KK, Aihara H *et al.* Differential assembly of Rous sarcoma virus tetrameric and octameric intasomes is regulated by the C-terminal domain and tail region of integrase. *J Biol Chem* 2018;293:16440–52. https://doi.org/10.1074/jbc.RA118.004768
14. Hare S, Gupta SS, Valkov E *et al.* Retroviral intasome assembly and inhibition of DNA strand transfer. *Nature* 2010;464:232–6. https://doi.org/10.1038/nature08784
15. Bhatt V, Shi K, Salamango DJ *et al.* Structural basis of host protein hijacking in human T-cell leukemia virus integration. *Nat Commun* 2020;11:3121. https://doi.org/10.1038/s41467-020-16963-6
16. Barski MS, Minnell JJ, Hodakova Z *et al.* Cryo-EM structure of the deltaretroviral intasome in complex with the PP2A regulatory subunit B56gamma. *Nat Commun* 2020;11:5043. https://doi.org/10.1038/s41467-020-18874-y
17. Yin Z, Shi K, Banerjee S *et al.* Crystal structure of the Rous sarcoma virus intasome. *Nature* 2016;530:362–6. https://doi.org/10.1038/nature16950
18. Pandey KK, Bera S, Shi K *et al.* Cryo-EM structure of the Rous sarcoma virus octameric cleaved synaptic complex intasome. *Commun Biol* 2021;4:330. https://doi.org/10.1038/s42003-021-01855-2
19. Ballandras-Colas A, Brown M, Cook NJ *et al.* Cryo-EM reveals a novel octameric integrase structure for betaretroviral intasome function. *Nature* 2016;530:358–61. https://doi.org/10.1038/nature16955
20. Jozwik IK, Li W, Zhang DW *et al.* B-to-A transition in target DNA during retroviral integration. *Nucleic Acids Res* 2022;50:8898–918. https://doi.org/10.1093/nar/gkac644
21. Passos DO, Li M, Jozwik IK *et al.* Structural basis for strand-transfer inhibitor binding to HIV intasomes. *Science* 2020;367:810–4. https://doi.org/10.1126/science.aay8015

Downloaded from https://academic.oup.com/nar/article/54/6/gkag270/8550793 by guest on 01 April 2026

22. Passos DO, Li M, Yang R *et al.* Cryo-EM structures and atomic model of the HIV-1 strand transfer complex intasome. *Science* 2017;355:89–92. https://doi.org/10.1126/science.aah5163
23. Cook NJ, Li W, Berta D *et al.* Structural basis of second-generation HIV integrase inhibitor action and viral resistance. *Science* 2020;367:806–10. https://doi.org/10.1126/science.aay4919
24. Li M, Yang R, Chen X *et al.* HIV-1 integrase assembles multiple species of stable synaptic complex intasomes that are active for concerted DNA integration *in vitro*. *J Mol Biol* 2024;436:168557. https://doi.org/10.1016/j.jmb.2024.168557
25. Deveryshetty J, Chadda R, Mattice JR *et al.* Yeast Rad52 is a homodecamer and possesses BRCA2-like bipartite Rad51 binding modes. *Nat Commun* 2023;14:6215. https://doi.org/10.1038/s41467-023-41993-1
26. Bera S, Shi K, Aihara H *et al.* Molecular determinants for Rous sarcoma virus intasome assemblies involved in retroviral integration. *J Biol Chem* 2023;299:104730. https://doi.org/10.1016/j.jbc.2023.104730
27. Kaushik V, Chadda R, Kuppa S *et al.* Fluorescent human RPA to track assembly dynamics on DNA. *Methods* 2024;223:95–105. https://doi.org/10.1016/j.ymeth.2024.01.019
28. Chadda R, Kaushik V, Ahmad IM *et al.* Partial wrapping of single-stranded DNA by replication protein A and modulation through phosphorylation. *Nucleic Acids Res* 2024;52:11626–40. https://doi.org/10.1093/nar/gkae584
29. Ingargiola A, Lerner E, Chung S *et al.* FRETBursts: an open source toolkit for analysis of freely-diffusing single-molecule FRET. *PLoS One* 2016;11:e0160716. https://doi.org/10.1371/journal.pone.0160716
30. Vacca J, Wai J, Fisher T *et al.* Discovery of MK-2048 - subtle changes confer unique resistance properties to a series of tricyclic hydroxypyrrole integrase strand transfer inhibitors. In *4th International AIDS Society (IAS) Conference, July 22-25, 2007*, Sydney Australia, 2007.
31. Pandey KK, Bera S, Vora AC *et al.* Physical trapping of HIV-1 synaptic complex by different structural classes of integrase strand transfer inhibitors. *Biochemistry* 2010;49:8376–87. https://doi.org/10.1021/bi100514s
32. Kulkosky J, Jones KS, Katz RA *et al.* Residues critical for retroviral integrative recombination in a region that is highly conserved among retroviral/retrotransposon integrases and bacterial insertion sequence transposases. *Mol Cell Biol* 1992;12:2331–8
33. Hohlbein J, Craggs TD, Cordes T. Alternating-laser excitation: single-molecule FRET and beyond. *Chem Soc Rev* 2014;43:1156–71. https://doi.org/10.1039/C3CS60233H
34. Pandey KK, Bera S, Zahm J *et al.* Inhibition of human immunodeficiency virus type 1 concerted integration by strand transfer inhibitors which recognize a transient structural intermediate. *J Virol* 2007;81:12189–99. https://doi.org/10.1128/JVI.02863-06
35. Smith SJ, Zhao XZ, Passos DO *et al.* Integrase strand transfer inhibitors are effective anti-HIV drugs. *Viruses* 2021;13:205. https://doi.org/10.3390/v13020205
36. Li M, Craigie R. Processing of viral DNA ends channels the HIV-1 integration reaction to concerted integration. *J Biol Chem* 2005;280:29334–9. https://doi.org/10.1074/jbc.M505367200
37. Valkov E, Gupta SS, Hare S *et al.* Functional and structural characterization of the integrase from the prototype foamy virus. *Nucleic Acids Res* 2009;37:243–55. https://doi.org/10.1093/nar/gkn938
38. Shi K, Pandey KK, Bera S *et al.* A possible role for the asymmetric C-terminal domain dimer of Rous sarcoma virus integrase in viral DNA binding. *PLoS One* 2013;8:e56892. https://doi.org/10.1371/journal.pone.0056892
39. Goodarzi G, Im GJ, Brackmann K *et al.* Concerted integration of retrovirus-like DNA by human immunodeficiency virus type 1 integrase. *J Virol* 1995;69:6090–7. https://doi.org/10.1128/jvi.69.10.6090-6097.1995
40. Sinha S, Pursley MH, Grandgenett DP. Efficient concerted integration by recombinant human immunodeficiency virus type 1 integrase without cellular or viral cofactors. *J Virol* 2002;76:3105–13. https://doi.org/10.1128/JVI.76.7.3105-3113.2002
41. Li M, Mizuuchi M, Burke TR, Jr *et al.* Retroviral DNA integration: reaction pathway and critical intermediates. *EMBO J* 2006;25:1295–304. https://doi.org/10.1038/sj.emboj.7601005
42. Miller MD, Farnet CM, Bushman FD. Human immunodeficiency virus type 1 preintegration complexes: studies of organization and composition. *J Virol* 1997;71:5382–90. https://doi.org/10.1128/jvi.71.7.5382-5390.1997

Downloaded from https://academic.oup.com/nar/article/54/6/gkag270/8550793 by guest on 01 April 2026

Received: September 9, 2025. **Revised:** February 17, 2026. **Accepted:** February 18, 2026
© The Author(s) 2026. Published by Oxford University Press.
This is an Open Access article distributed under the terms of the Creative Commons Attribution-NonCommercial License (https://creativecommons.org/licenses/by-nc/4.0/), which permits non-commercial re-use, distribution, and reproduction in any medium, provided the original work is properly cited. For commercial re-use, please contact reprints@oup.com for reprints and translation rights for reprints. All other permissions can be obtained through our RightsLink service via the Permissions link on the article page on our site—for further information please contact journals.permissions@oup.com.